Application of the transferred matrix method to a unified evaluation of the cathodic electron emission

Cite as: AIP Advances **8**, 085322 (2018); https://doi.org/10.1063/1.5041314
Submitted: 24 May 2018 • Accepted: 20 August 2018 • Published Online: 28 August 2018

M. Baeva

Application of the transferred matrix method to a unified evaluation of the cathodic electron emission

M. Baeva[a]
Leibniz Institute for Plasma Science and Technology, Felix-Hausdorff-Str. 2, 17489 Greifswald, Germany

(Received 24 May 2018; accepted 20 August 2018; published online 28 August 2018)

The work is concerned with the Transfer Matrix Method for solving the steady-state Schrödinger equation applied for a unified evaluation of the emission current density from non-refractory cathodes. The method is applicable to arbitrary shapes of the potential barrier and its transmission probability is obtained without any analytical approximations. The Fermi-Dirac distribution for the free electrons in the metal is considered as a supply function. The results, obtained for a work function of the cathode material of 4.5 eV over a wide range of values of the surface temperature and the electric field strength, clearly show a growing deviation from those obtained by the classical Jeffreys-Wentzel-Kramers-Brillouin approximation with the increase of the electric field strength. Preliminary results are obtained to demonstrate the applicability of the Transfer Matrix method to the evaluation of the ion-assisted electron emission. A significant local enhancement of the emission current density is obtained as a result of the presence of an ion at a fixed position near the metal surface. The effect becomes very strongly pronounced at an appropriate value of the electric field strength, for which a resonant ion contribution appears. https://doi.org/10.1063/1.5041314

I. INTRODUCTION

The interaction between an electric arc and its electrodes has become a basic feature of up-to-date arc plasma models due to the need for understanding and describing the arc attachment to the electrodes. Various aspects of the arc attachment to refractory cathodes and non-refractory anodes has been presented in review articles during the last decade (see e.g. Refs. 1–4). Refractory cathodes withstand temperatures above the melting point of non-refractory materials and the emission current from them is chiefly due to thermionic emission. Non-refractory cathodes, as used e.g. in gas-metal welding arcs, circuit breakers, and plasma torches, have been considered to produce electron emission due to the high electric field near the cathode surface.[5] Although it was also proposed that instead of field emission, electrons may be produced as a result of photoionization of neutral atoms by radiation from the arc[6] or impact of excited atoms at the cathode,[7] the dominant emission mechanism has not been clearly established. It has been shown by Ecker et al.[8] that the thermo-field emission current can be significantly enhanced by the field of ions coming from the plasma without having to enhance the temperature or the electric field at the cathode surface. Coulombe et al.[9] presented a numerical model of the arc attachment on a non-refractory cathode considering the pressure build up in the cathode region due to vaporization of the cathode material and the ion-enhanced thermo-field emission of electrons. The physically justified and numerically accurate evaluation of the electron emission current is of central importance to the modelling of the arc attachment on non-refractory cathodes.

Thermionic and field emission have been the subject of separate studies for a long time (see Ref. 10 and the references therein) and are generally well understood in the frame of relatively

[a]Electronic mail: baeva@inp-greifswald.de

simple models.[11,12] Thermo-field emission from a metallic surface has been considered by Paulini et al.[13] for a wide range of temperatures, field strengths and work function values of the emitter. The authors have given the ranges of validity of known approximations and have shown that simplified formulae of the Fowler-Nordheim approximation may give incorrect results to several orders of magnitude. The authors proposed easy-to-use formulae for numerical modelling of arc cathode spots. A method of a computationally efficient evaluation of the emission current density in the range of validity of the Murphy-Good theory has been presented by Benilov et al.[14] These methods, however, do not take into account the ion contribution.

Numerical calculations of the electron emission current using the Numerov integration of the Schrödinger eigenvalue equation are presented by Teste et al. and Gayet et al.[15,16] Spataru et al.[17] extended the study[16] to a three-dimensional one. These calculations eliminate the Jeffreys-Wentzel-Kramers-Brillouin (JWKB) approximation (which is an expansion at zeroth order of the wavefunction argument) and gives the corrections that have to be applied to the Richardson,[18] Fowler-Nordheim[19] or Murphy and Good[11] results. This approach also allows one to consider the ion-enhanced thermo-field emission of electrons. The calculated amplification coefficients for an electric field strength of 10^9 V/m by Gayet et al.[16] are used by Coulombe et al.,[9] and a comparison of the electron-emission equations is given. Furthermore, Coulombe et al.[9] report the important role of the ion enhancement in particular at temperatures above 2000 K and electric field above 10^9 V/m.

An alternative to the Numerov method suggests the Transferred Matrix Method (TMM) with which the present work is concerned. The TMM has been applied to the case of a combined field and thermionic emission[20] from a copper knife-edge cathode at a temperature of 330 °C in an ultrahigh vacuum chamber. The results showed a very significant nonzero temperature contributions leading to a strong deviations from the predictions based on the Fowler-Nordheim equation. To the best of author's knowledge, the TMM has not been yet applied to obtain the electron emission current density from non-refractory arc cathodes in account for ion enhancement. In this work, the TMM is considered in order to explore its capability of predicting the current density of electron emission under conditions relevant to arc discharges. An arbitrary potential barrier, which implies the contributions from the applied electric field, perturbations induced by the image charge of the released electron and the presence of an ion as a first approximation. Furthermore, in comparison to work,[20] special care has been taken to describe the electron-surface interaction[21] and a more efficient numerical algorithm[22] has been implemented. The paper is organized as follows. The section II presents theory basics and the evaluation procedure, selected results are shown in the section III, and concluding remarks are given in the section IV.

II. THEORETICAL BACKGROUND

The current density of electrons emitted from a metal surface at a temperature T_c at the presence of electric field F can be expressed as[10]

$$J_{em} = e \int_{-\infty}^{\infty} \int_{W_a}^{E} T(F, W) \mathcal{N}(T_c, \phi, E) dW dE, \tag{1}$$

where

$$\mathcal{N}(T_c, \phi, E) = \frac{4\pi m_e}{h^3} \left(\exp\left(\frac{E+\phi}{k_B T_c} \right) + 1 \right)^{-1} \tag{2}$$

is the electron supply function, which is expressed by the Fermi-Dirac distribution for the free electrons in the metal according to the Sommerfeld theory, ϕ is the work function of the material, W is the electron energy corresponding to the motion normal to the surface, and E is the total energy. The quantity $T(F, W)$ is the transmission probability that an electron incident on the surface potential barrier emerges the metal.

Figure 1 shows a schematic representation of an emitted electron, a singly charged ion at some distance from the metal surface, and their image charges at given instant. The metal surface is assumed to be smooth and plane. The cylindrical system of reference is chosen so that the Z-axis is going through the ion and its image. The emitted electron lies off-side the Z-axis by a distance ρ.

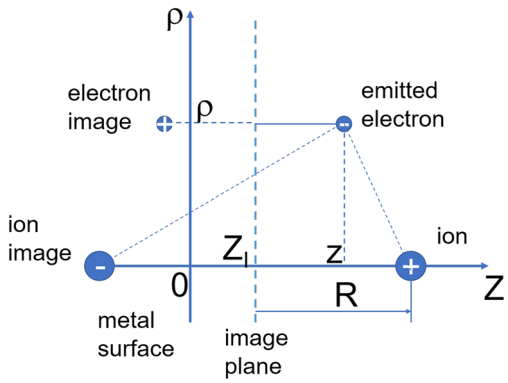

FIG. 1. Schematic of the metal surface with an escaped electron and its image, an ion at some distance from the surface and its image charge.

The effective position of the metal surface, i.e. the shift of the image plane, is denoted as Z_I. The z-dependence of the problem is followed as a first approximation. Such consideration is physically reasonable and unambiguous for the purpose followed in this work. This purpose is a preliminary study in regard to a model of the space-charge sheath of a non-refractory cathode, which in general is one-dimensional and considers the direction perpendicular to the cathode.

The potential that the emitted electron experiences is considered in units of *SI* in account for the contributions of

- the external electric field F

$$V_1(z) = -Fz, \text{ if } z \geq 0, \tag{3}$$

- the force of the electron image on the electron

$$V_2(z) = \begin{cases} -\dfrac{V_0/e}{A\exp[B(z-Z_I)]+1}, & \text{if } z \leq Z_I \\ -\dfrac{e}{4\pi\varepsilon_0}\dfrac{1-\exp[-\lambda(z-Z_I)]}{4(z-Z_I)}, & \text{if } z > Z_I \end{cases} \tag{4}$$

- the force of the ion on the electron

$$V_3(\rho,z) = -\frac{e}{4\pi\varepsilon_0}\frac{1}{\sqrt{\rho^2+[z-(R+Z_I)]^2}}, \text{ if } z > Z_I \tag{5}$$

- the force of the ion image on the electron

$$V_4(\rho,z) = \frac{e}{4\pi\varepsilon_0}\frac{1}{\sqrt{\rho^2+[z+(R-Z_I)]^2}}, \text{ if } z > Z_I. \tag{6}$$

With account of equations (3)–(6), the potential $V(\rho, z)$ is given by

$$V(\rho,z) = V_1(z) + V_2(z) + V_3(\rho,z) + V_4(\rho,z). \tag{7}$$

The term $V_2(z)$ in Eq. (4) is written in a way which avoids the singularity at $z = Z_I$ and matches the constant potential $W_a = -V_0$ inside the metal according to the jellium description.[16,21] Notice that such treatment has not been done in the work.[20] As further parameters, $Z_I \sim a_0$ is the shift of the image plane, a_0 is the Bohr radius, R is the distance of the ion from the image plane, λ is a characteristic of the metal (e.g. V_0=11.2 eV, λ=1.05/a_0 for copper), $A = \frac{4\pi\varepsilon_0}{e^2}\frac{4V_0}{\lambda} - 1$, $B = \frac{4\pi\varepsilon_0}{e^2}\frac{2V_0}{A}$.

For a long distance z from the metal surface, the potential energy is dominated by the electric field contribution V_1 (line 1 in Fig. 2). The addition of the contribution of the electron image leads to the "Schottky-Nordheim" barrier (curve 2 in Fig. 2), while the full expression of $V(\rho, z)$ in Eq. (7) results in a complex barrier structure (curve 3 in Fig. 2). The calculation of the transmission

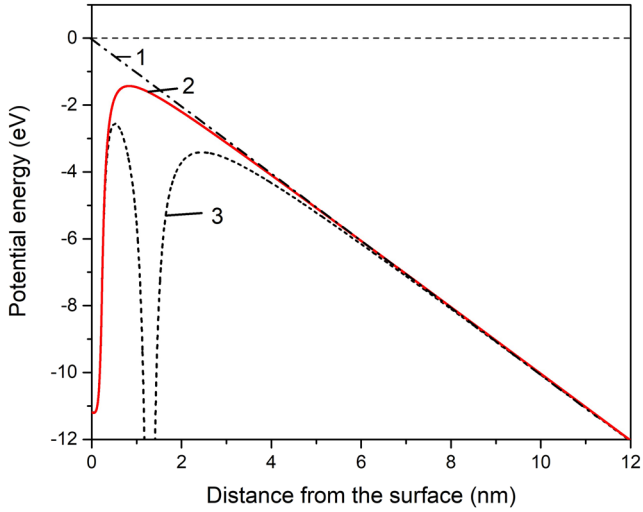

FIG. 2. Potential barrier for an emitted electron near the surface with account for the terms 1) V_1, 2) $V_1 + V_2$, 3) $V_1 + V_2 + V_3 + V_4$, and parameters of the potential barrier: F=10^9 V/m, V_0=11.2 eV, ρ=1a_0, R=20a_0.

probability is described below following the computational algorithm by Gilmore.[22] The stationary one-dimensional Schrödinger equation

$$\frac{d^2\psi(z)}{dz^2} = -\frac{2m_e}{\hbar^2}(W - V(z))\psi(z) \tag{8}$$

for the wavefunction of an electron with energy W in a potential $V(z)$ is employed. For an electron incident at the boundary at $z = a$ between region 1 and region 2 (see Fig. 3), the solution can be expressed as a linear superposition of the two particular solutions $\psi_1(z)$, $\psi_2(z)$, which depend on whether the term $-\frac{2m_e}{\hbar^2}(W - V(z))$ is negative, zero or positive:

$$\begin{aligned}
&\psi_1 = \exp(+ikz), \quad \psi_2 = \exp(-ikz), \quad \text{if } -\tfrac{2m_e}{\hbar^2}(W - V(z)) = -k^2 < 0,\\
&\psi_1 = 1, \qquad\qquad \psi_2 = z, \qquad\qquad \text{if } -\tfrac{2m_e}{\hbar^2}(W - V(z)) = 0,\\
&\psi_1 = \exp(-kz), \quad \psi_2 = \exp(+kz), \quad \text{if } -\tfrac{2m_e}{\hbar^2}(W - V(z)) = k^2 > 0,
\end{aligned} \tag{9}$$

and

$$\psi(z) = \begin{cases} A_1\psi_1(z) + B_1\psi_2(z), & \text{if } z \le a \\ A_2\psi_1(z) + B_2\psi_2(z), & \text{if } z \ge a. \end{cases} \tag{10}$$

The first derivative of the wavefunction can be expressed similarly so that the matrix relation between the wavefunction, its first derivative, and the coefficients A_j, B_j (j = 1, 2) for region 1 and region 2 can be introduced

$$\begin{pmatrix} \psi(z) \\ \psi'(z) \end{pmatrix} = \begin{pmatrix} \psi_1(z) & \psi_2(z) \\ \psi_1'(z) & \psi_2'(z) \end{pmatrix} \begin{pmatrix} A_j \\ B_j \end{pmatrix}. \tag{11}$$

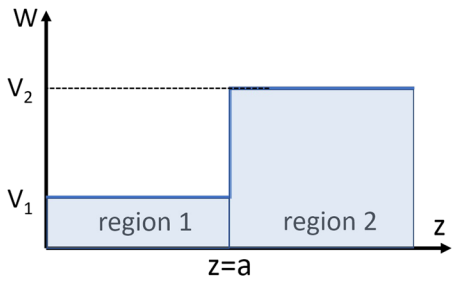

FIG. 3. Schematic of the step structure. The wavefunction and its first derivative are matched at the boundary $z = a$.

Matching the wavefunction and its first derivative at the boundary $z = a$ (Fig. 3), we can write the following matrix equation without any assumptions about the relative values of the particle energy W and the heights of the potential barrier V_1 and V_2

$$\begin{pmatrix} A_1 \\ B_1 \end{pmatrix} = \mathcal{T}_{12} \begin{pmatrix} A_2 \\ B_2 \end{pmatrix}, \tag{12}$$

where $\mathcal{T}_{12} = \mathcal{E}^{-1}(V_1, a)\mathcal{K}^{-1}(V_1)\mathcal{K}(V_2)\mathcal{E}(V_2, a)$ is the 2x2 transfer matrix and $\mathcal{K}, \mathcal{E}$ are 2x2 matrices ($\mathcal{K}^{-1}, \mathcal{E}^{-1}$ are their inverses), which can be easily expressed for the three cases given in Eqs. (9). For a piecewise constant potential energy with $N - 1$ breakpoints, the relationship between (A_1, B_1) and (A_N, B_N) reads

$$\begin{pmatrix} A_1 \\ B_1 \end{pmatrix} = \mathcal{T}_{12}\mathcal{T}_{23} \ldots \mathcal{T}_{N-1,N} \begin{pmatrix} A_N \\ B_N \end{pmatrix} = \mathcal{T} \begin{pmatrix} A_N \\ B_N \end{pmatrix} \tag{13}$$

The computation of the transferred matrix involves the product of $N - 2$ matrices according to Eq. (13) and 2×2 matrices on the two boundaries resulting in $N + 2$ matrices. Notice that the present approach is computationally more efficient and it differs from that by He et al.,[20] where the potential barrier was divided into a number of finite square barriers and the plain matrix treatment involves the product of at least $3N$ matrices. Taking into account that a particle is incident from the left ($A_1 \neq 0$) but not from the right ($B_N = 0$), and the conservation of momentum[22]

$$\hbar k_1 \left(|A_1|^2 - |B_1|^2 \right) = \hbar k_N \left(|A_N|^2 - |B_N|^2 \right), \tag{14}$$

the following relation can be derived

$$\left| \frac{B_1}{A_1} \right|^2 + \frac{k_N}{k_1} \left| \frac{A_N}{A_1} \right|^2 = 1. \tag{15}$$

The first term on the left-hand side of Eq. (15) has the meaning of reflection probability, while the second represents the transition probability. The latter can be expressed by means of the corresponding element t_{11} of the transfer matrix $\mathcal{T}$

$$T = \frac{k_N}{k_1} \left| \frac{1}{t_{11}} \right|^2. \tag{16}$$

The emission current density is finally obtained from Eq. (1), the supply function $\mathcal{N}$ from Eq. (2), and the transition probability is obtained by the TMM from Eq. (16).

III. RESULTS AND DISCUSSION

The number of breakpoints of the potential barrier used in the computation varies from 2×10^4 up to 1×10^6 and depends on the electric field strength. A larger number of breakpoints is needed at a weaker electric field for which the potential barrier is thicker. The code is realized in MATLAB. Calculations have been carried out at conditions reported by Gayet et al.[16] in order to compare the results of the TMM with that based on the Numerov integration of the Schrödinger eigenvalue equation. The results obtained showed that the TMM can reproduce the results by Gayet et al.[16]

The transmission probability calculated according to the JWKB approximation, applied by Murphy and Good,[11] and the TMM is shown in Figure 4 for two values of the electric field strength. For electron energies larger than $W_l = -\sqrt{\frac{e^3 F}{8\pi\varepsilon_0}}$, the transition probability in the approach by Murphy and Good is set to one, while the TMM predicts a smooth increase to one. For an electric field of 10^9 V/m, the TMM and JWKB transition probabilities are almost equal below electron energy of approximately $W_l \simeq$-0.84 eV. The difference is more pronounced for an electric field of 10^{10} V/m, for which $W_l \simeq$-2.7 eV.

Figure 5 shows the change of the potential barrier with the field strength and the influence of an ion located at some distance from a clean and smooth copper surface (R=20a_0, V_0=11.2 eV, $\lambda = a_0^{-1}$). The increase in the electric field leads to a lowering and narrowing of the potential barrier. In the presence of an ion, the electron will feel two successive potential barriers. We notice the

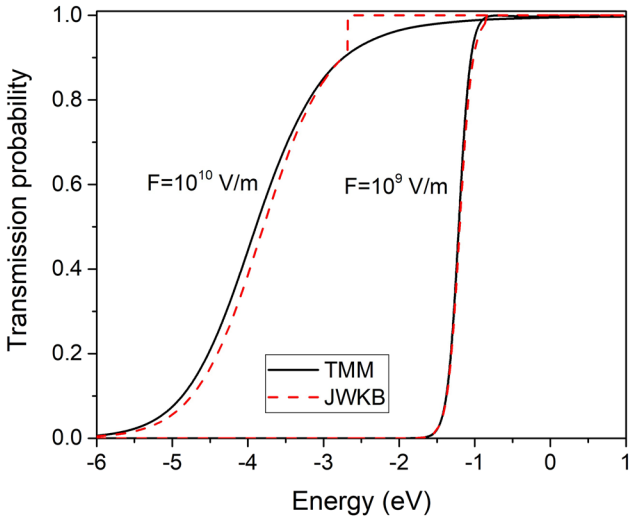

FIG. 4. Transmission probability for electron emission without ion contribution at electric field of 10^9 and 10^{10} V/m obtained by means of the TMM and the JWKB approximation. V_0=11.2 eV, ρ=1a_0.

different height especially of the right wing of the second part of the potential barrier depending on the electric field strength. While the height of the right wing is even higher than the left one for F=10^7 V/m or comparable with the left one for F=10^8 V/m, it becomes slightly lower for F=10^9 V/m and significantly lower for F=10^{10} V/m. This effect is highly important for the transmission probability of an electron through the potential barrier as it is shown below.

From the theoretical background of the TMM given above in the framework of the one-dimensional treatment, it is clear that the method avoids any analytical approximation in the calculation of the transmission probability. Therefore, the emission current density is obtained in a unified way no matter whether the emission is of thermionic, thermo-field or field nature. At zero and low electric field strengths, the thermionic and the thermo-field emission current density is well predicted by the Richardson-Dushmann-Schottky equation

$$J_R = e\frac{4\pi m_e k_B^2 T_c^2}{h^3}\exp\left(-\frac{e(\phi-\Delta\phi)}{k_B T_c}\right). \tag{17}$$

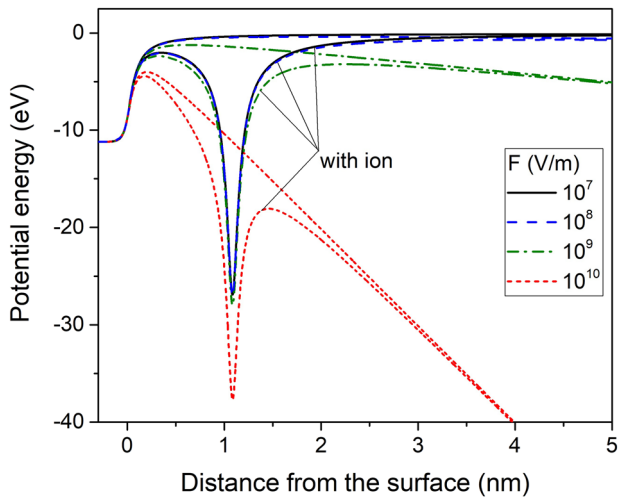

FIG. 5. Potential barrier for an electron near the surface for various values of the electric field. V_0=11.2 eV, ρ=1a_0, R=20a_0.

In Eq. (17), $\Delta\phi = \sqrt{\frac{eF}{4\pi\varepsilon_0}}$ is the lowering of the work function due to the Schottky effect. The Schottky correction $\Delta\phi$ has to be small compared to the work function in order to consider Eq. (17) as still valid. The electron emission described with Eq. (17) is usually referred to as the field-enhanced thermionic emission.

Figure 6 shows the ratio between the emission current densities J_{TMM} and J_{JWKB} obtained by means of the TMM-approach and the JWKB-approximation, respectively, and the value J_R for electric field strengths F= 10^7, 10^8, 10^9, and 10^{10} V/m and surface temperatures from 1000 K up to 6000 K. In these results, the ion contribution to the change of the potential barrier is not taken into account in J_{TMM} for the sake of the comparison with J_{JWKB}. The ratios J_{TMM}/J_R (line with squares) and J_{JWKB}/J_R (line with circles) are close to one for temperatures from 1000 K up to 6000 K and electric field strength 10^7 and 10^8 V/m. For electric field of 10^9 V/m, the values of J_{TMM} and J_{JWKB} are close to each other as it can be expected from the almost equal transmission probabilities (Fig. 4). However, the ratios J_{TMM}/J_R and J_{JWKB}/J_R considerably increase in particular for temperatures between 1000 K and 2000 K. This shows that Eq. (17) significantly underestimates the emission current density for

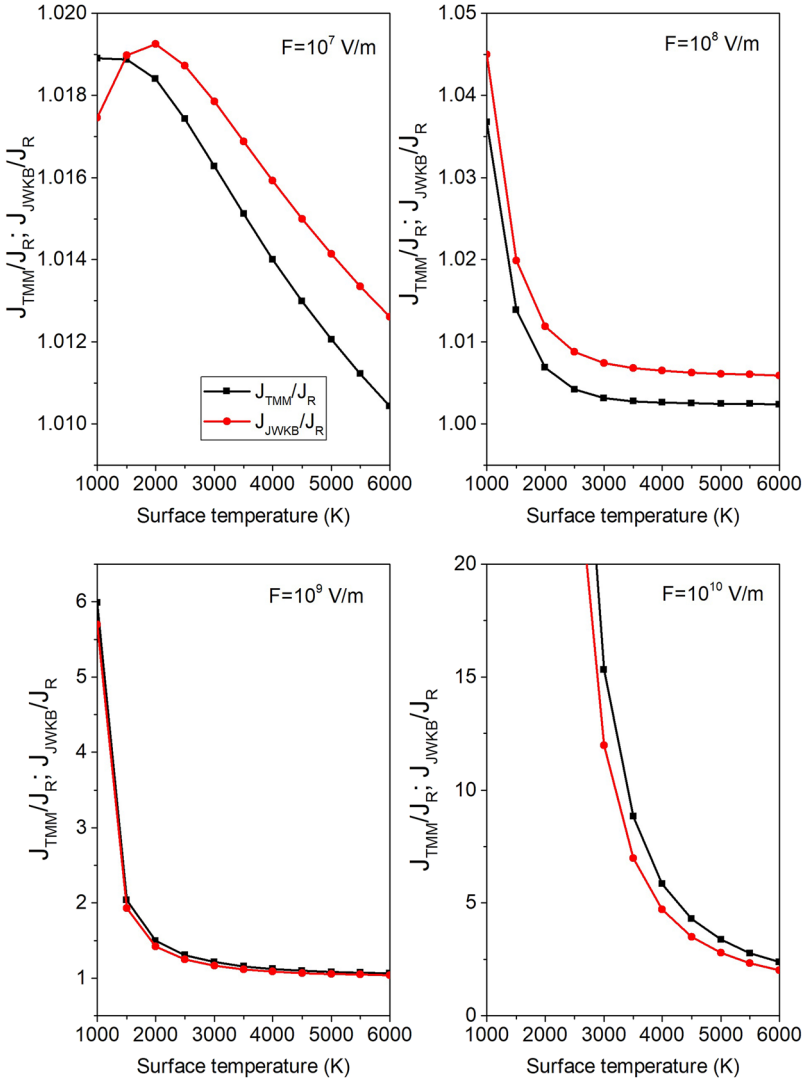

FIG. 6. Ratios between the emission current obtained by means of the TMM without ion contribution and the JWKB approximation and the emission current from the Richardson-Schottky theory. J_{TMM}/J_R - line with square symbols, J_{JWKB}/J_R - line with circles.

such conditions. For electric field of 10^{10} V/m and above, the difference between J_{TMM} and J_{JWKB} becomes more pronounced.

It is clear from Eq. (7) with account of equations (3)–(6), that the shape of the potential barrier changes for variations of the ion position. That is, the ions are moving towards the cathode so that the distances R and ρ in general change. The elementary volume occupied by an ion at given ion density n_i can be estimated as $V = \frac{1}{n_i} \sim \rho_{max}^2 \times R_{max}$. The one-dimensional potential barrier at fixed ρ and R certainly differs from the real one. Nevertheless, it allows one to prove the applicability of the TMM and to study the effect of the ion assistance before going to a multidimensional treatment. In what follows, we discuss the impact of the ion presence at a given position from the metal on the transmission probability and the emission current density for various electric field strengths. The parameters of the study (ρ=1a_0, R=20a_0, V_0=11.2 eV, F=10^7 –10^{10} V/m) are the same used in Fig. 5. As shown in Fig. 4, the ion presence, on the one hand, lowers the potential barrier. On the other hand, the potential barrier is split into two tinner parts. The transmission probability, T, calculated with and without the ion contribution is shown in Fig. 7 for several values of the electric field strength. The region of transmission probability values T=0.95-1 is enlarged in order to show the nonmonotonic, weakly oscillating behaviour at high electron energy, which appears due to the wavelike reflection of electrons. The transmission probability increases with the increase of the electric field strength both with and without the presence of the ion. This is due to the lowering of the potential barrier. While the increase is progressive in the case without ion, it is slowed down beyond F=10^9 V/m when an ion is present. This effect can be explained with the change of the potential barrier shown in Fig. 5. The potential barrier changes dramatically for F=10^{10} V/m in comparison with F=10^9 V/m. In particular, the height of the second part of the barrier is significantly lower than that of the first one. As a result, the transmission probability is mainly due to the tunnelling through the first barrier. The latter is tinner in the case an ion is present. The transmission probability increases due to the ion presence but this increase is moderate in comparison with that at F=10^9 V/m.

At an electric field F=10^9 V/m, a further effect occurs. A sharp peak in the transition probability is obtained at the energy of about -3.46 eV. This effect is attributed to the resonance contribution[16,17] which corresponds to the formation of quasi-stationary states of the neutral species. The latter are built due to the trapping of the emitted electron in the potential well of the ion. The neutralization of the ion is followed by ionization in the macroscopic electric field. The success of the process chain $A^+ + e \rightarrow A^* \rightarrow^F A^+ + e$ depends on the availability of atomic states near the Fermi-level of the metal. As an example, excited states of argon, which is frequently used in arc discharges, lie in the

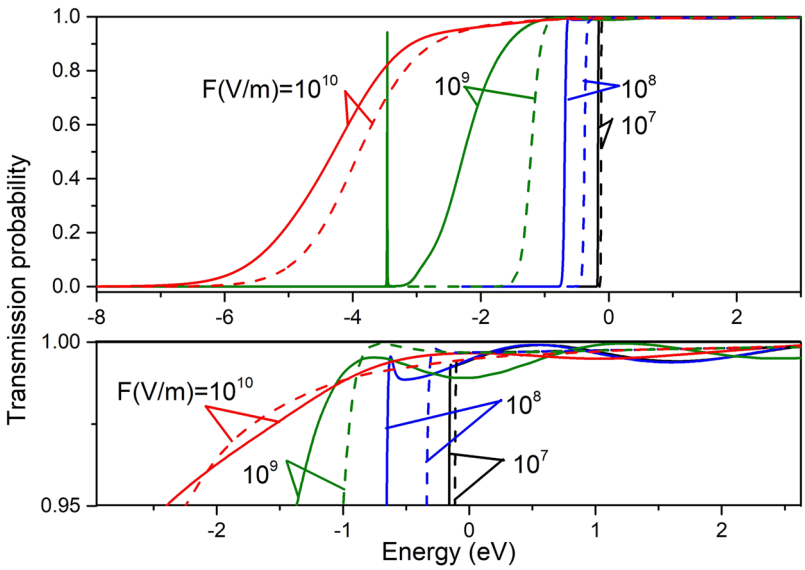

FIG. 7. Transmission probability of the potential barrier for various electric field strength with (solid curves) and without (dash curves) ion contribution.

energy range with a width of about 4.3 eV (the difference between the ionization energy of ~15.8 eV and the energy of the first excited state ~11.5 eV). The excited states of the atom can therefore be easily ionized, which enables the tunnelling effect for energies below the top of the second part of the potential barrier. The electron emission can be considered as a sequence of an electron tunnelling through the first part of the barrier followed by the trapping in the potential well with a formation of an excited atom, which in the row becomes ionized, followed by the tunnelling of the electron through the second part of the potential barrier. In this context, the atomic states are "pumping" electrons into the plasma.

In order to demonstrate the impact of the ion contribution on the current density of the emitted electrons, the dimensionless part of the integrand in Eq. (1) is plotted in Fig. 8. It represents the product of the transmission probability T and the temperature-dependent multiplier $\tilde{\mathcal{N}} = \left[\exp\left(\frac{E+\phi}{k_B T_c}\right) + 1\right]^{-1}$ in the supply function in Eq. (2). The results are obtained for electric field strength F=10^9 V/m and surface temperatures T_c=1000 K, 2000 K, and 3000 K. The $T\tilde{\mathcal{N}}$-values increase rapidly with the increase of the surface temperature. In particular, in the absence of an ion, the increase is of many orders of magnitude when the temperature is increased from 1000 K to 2000 K. In the presence of an ion, the maximum $T\tilde{\mathcal{N}}$-values are shifted to lower values of the electron energy. The sharp peaks correspond to the resonant part of the ion contribution. Notice the logarithmic scale of the graph which visualizes the weaker second peak of the resonant ion contribution at electron energy slightly above -4.5 eV (not evident in Fig. 8).

In consideration of the above, the presence of an ion close to the metal surface leads to an enhancement of the emission current density. The local enhancement factor denotes the ratio between the emission current density in the presence of an ion and the emission current density obtained with no account of an ion for the given values of ρ and R. This factor is presented in Fig. 9 for the parameters used in the present work, i.e. ρ=1a_0 and R=20a_0. The local enhancement factor is in particular large at lower surface temperatures. This agrees with the results in Figs. 7 and 8. Indeed, in the presence of an ion, the transmission probability increases with the increase of the electric field strength, and the $T\tilde{\mathcal{N}}$-values increase with the increase of the surface temperature even if no resonant ion contribution appears. The local enhancement factor becomes extremely large at low surface temperatures and electric field strengths, at which the resonant contribution appears. This is for example the case T_c=1000 K and F=10^9 V/m under the conditions ρ=1a_0 and R=20a_0. The local enhancement factor decreases with the increase of the surface temperature since the difference between the $T\tilde{\mathcal{N}}$-values progressively decreases. It is worth noting that a non-refractory cathode cannot withstand surface temperatures above say 2000 K.

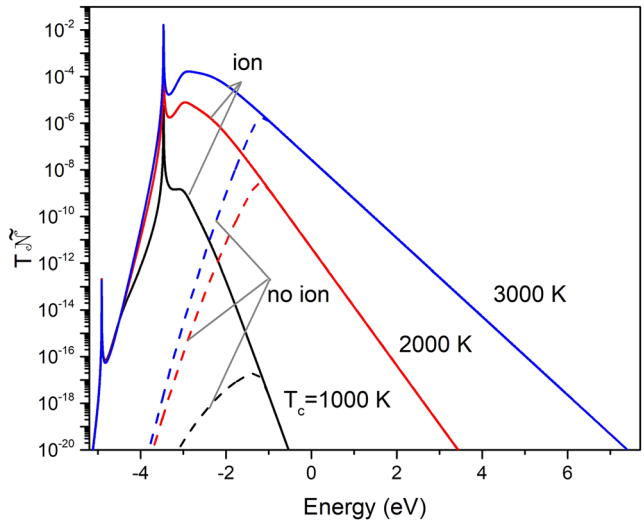

FIG. 8. The product $T\tilde{\mathcal{N}}$ as a function of the electron energy for F=10^9 V/m and various temperatures of the metal surface with and without ion contribution.

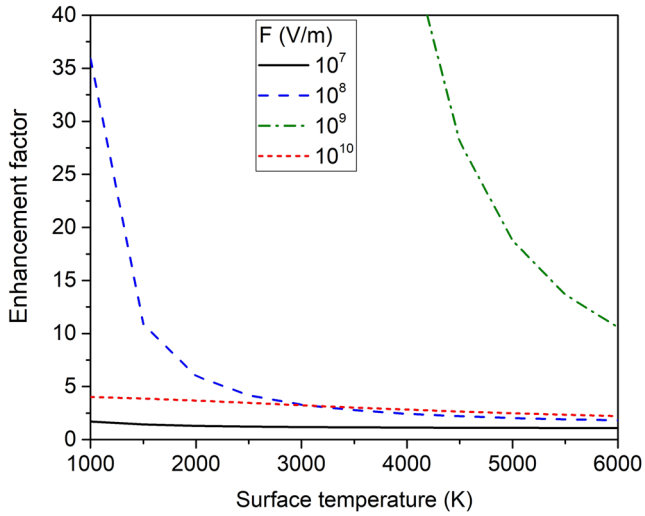

FIG. 9. The local enhancement factor of the thermo-field emission current due to the ion contribution versus the surface temperature for various electric field strengths. The results are obtained by means of the TMM with ρ=1a_0, R=20a_0.

The present results demonstrate the effect of the ion-assisted electron emission for fixed parameters ρ and R. In order to obtain an average enhancement factor, appropriate averaging over ρ and R is further needed (e.g. as it has been done in Ref. 16). Future activities will consider this aspect in regard to a model of the space-charge sheath of non-refractory cathodes.

IV. CONCLUSION

In the present work, we demonstrated the applicability of the TMM for the accurate calculation of the transmission probability of an electron through an one-dimensional potential barrier of an arbitrary shape. The TMM enables a unified evaluation of the thermo-field and ion-assisted electron emission from a clean and smooth copper surface. The approach does not make use of any analytical approximations concerning the shape of the barrier. The evaluation predicts an emission current density at low electric field in agreement with the approach by Murphy and Good. It is applicable to cases of high electric field and in the presence of an ion near the cathode surface. The presence of an ion close to the metal surface leads to a significant local enhancement of the emission current especially at low temperatures. For a fixed position of the ion, a resonant ion contribution appears at a given electric field strength and leads to an increase of the local enhancement factor in several orders of magnitude. Future works related to the space-charge sheath of non-refractory cathodes will use this evaluation procedure.

[1] M. S. Benilov, J. Phys. D: Appl. Phys. **41**(30pp), 144001 (2008).
[2] J. Heberlein, J. Mentel, and E. Pfender, J. Phys. D: Appl. Phys. **43**, 023001 (2010).
[3] J. Mentel and J. Heberlein, J. Phys. D: Appl. Phys. **43**, 023002 (2010).
[4] S. M. Shkol'nik, Plasma Sources Sci. Technol. **20**, 013001 (2011).
[5] T. H. Lee, J. Appl. Phys. **30**, 166 (1959).
[6] J. J. Lowke, J. Phys. IV France **7**, 283 (1997).
[7] J. J. Lowke and M. Tanaka, Proc. 17th Int. Conf. on Gas Discharges and Their Applications **7**, 137 (2008).
[8] G. Ecker and K. G. Müler, J. Appl. Phys. **30**, 1466 (1959).
[9] S. Coulombe and J.-L. Meunier, J. Phys. D: Appl. Phys. **30**, 2905 (1997).
[10] A. Anders, *Cathodic arcs: From fractal spots to energetic condensation* (Springer, 2008).
[11] E. L. Murphy and R. H. Good, Phys. Rev. **102**, 1464 (1956).
[12] S. G. Christov, Phys. Stat. Sol. **17**, 11 (1966).
[13] J. Paulini, T. Klein, and G. Simon, J. Phys. D: Appl. Phys. **26**, 1310 (1993).
[14] M. S. Benilov and L. G. Benilova, J. Appl. Phys. **114**, 063307 (2013).
[15] P. Teste and J.-P. Chabrerie, J. Phys. D: Appl. Phys. **29**, 697 (1996).
[16] R. Gayet, C. Harel, T. Josso, and H. Jouin, J. Phys. D: Appl. Phys. **29**, 3063 (1996).
[17] C. Spataru, D. Teillet-Billy, P. Teste, and J. P. Chabrerie, J. Phys. D: Appl. Phys. **30**, 1135 (1997).
[18] O. W. Richardson, *The emission of electricity from hot bodies* (Longmans Green and Company, 1921).

[19] R. H. Fowler and L. Nordheim, Proc. R. Soc. Lond. A **119**, 173 (1928).
[20] X. He, J. Scharer, J. Booske, and S. Sengele, J. Vac. Sci. Technol. **B26**, 770 (2008).
[21] P. J. Jennings, R. O. Jones, and M. Weinert, Phys. Rev. B **37**, 6113 (1988).
[22] R. Gilmore, *Elementary quantum mechanics in one dimension* (The John Hopkins University Press, 2004).